A01-31404

AIAA 2001–2900

Particle and Continuum Computations of Hypersonic Flow Over Sharp and Blunted Cones

Wen-Lan Wang and Iain D. Boyd
Aerospace Engineering
University of Michigan, Ann Arbor, MI 48109

Graham V. Candler and Ioannis Nompelis
Aerospace Engineering and Mechanics & Army HPC Research Center
University of Minnesota, Minneapolis MN 55455

35th AIAA Thermophysics Conference
June 11–14, 2001/Anaheim, CA

Particle and Continuum Computations of Hypersonic Flow Over Sharp and Blunted Cones

Wen-Lan Wang* and Iain D. Boyd†
Aerospace Engineering
University of Michigan, Ann Arbor, MI 48109
Graham V. Candler‡ and Ioannis Nompelis§
Aerospace Engineering and Mechanics & Army HPC Research Center
University of Minnesota, Minneapolis MN 55455

Abstract

An extensive numerical study of hypersonic flow around axisymmetric cones is conducted using particle and continuum methods. A number of accuracy issues are carefully investigated for the particle method, including grid sensitivity, time convergence and accommodation coefficient. Flow field comparisons between the particle and continuum methods are provided. The comparisons of computational solutions and experimental data along the cone surface are also presented. The particle simulations provide good agreement with the measured data. It is shown that the temperature used to evaluate the thermal conductivity in the heat transfer expression for the continuum method has a large effect on the prediction of heat transfer rate.

Introduction

The interaction of the bow shock of a hypersonic vehicle and the shock waves from a wing or control surface are of great interest in space vehicle design because of the potentially high localized temperature and the associated extremely high heating rates in the interaction region. Due to the tremendous technical difficulties and costs in obtaining laboratory and flight measurements under realistic conditions, numerical methods play an important role in the design of new hypersonic vehicles.

In prior work, it has been found that the flow about a double cone model is very challenging to various numerical methods. A schematic of this configuration is shown in Fig. 1. Despite its simple shape, a double cone creates complicated flow structures. In general, the first cone produces an attached oblique shock wave, and the second, larger angle cone produces a detached bow shock. These two shock waves interact to form a transmitted shock that strikes the second cone surface near the cone-cone juncture. The adverse pressure gradient due to the cone juncture configuration and the transmitted shock generates a large region of separated flow that in turn produces its own separation shock. This shock interacts with the attached oblique shock from the first cone, altering the interaction with the detached shock from the second cone. The size of the separation region is then affected by this interaction. Reference 1 demonstrates this kind of complex flow structure by solving the Navier-Stokes (NS) equations numerically while Ref. 2 illustrates similar behavior by utilizing the direct simulation Monte Carlo (DSMC) method.[3]

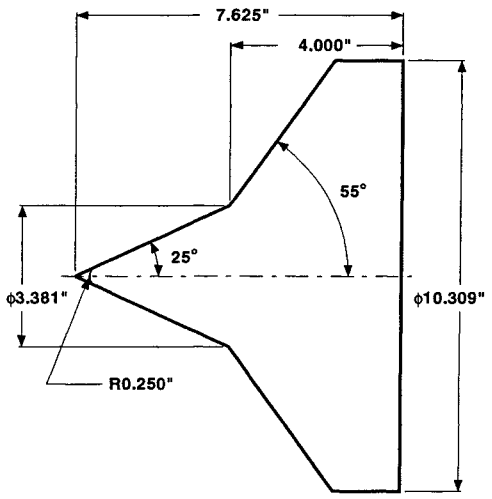

Fig. 1 Schematic of the 25°-55° sharp and blunted double-cone wind-tunnel models.

In order to have an opportunity to compare numerical results and experimental data, a hypersonic

*Graduate Student Research Assistant, Student Member AIAA
†Associate Professor, Senior Member AIAA
‡Professor,Senior Member AIAA
§Graduate Research Assistant, Student Member AIAA

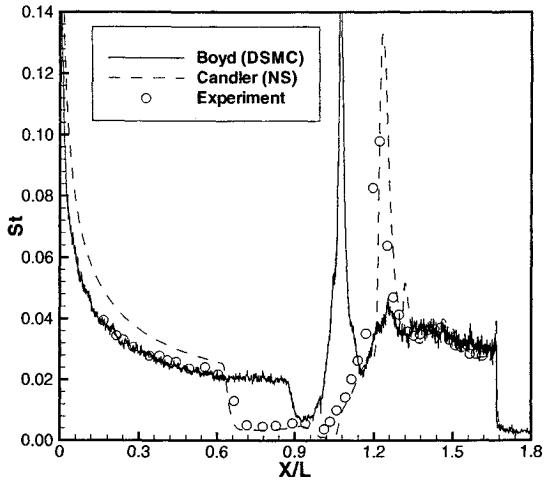

Fig. 2 Comparison of surface heat transfer coefficient for Run 35[10] on the 25°-55° sharp double-cone wind-tunnel model.

code validation exercise was organized by Dr. Michael Holden in January 2001. The exercise consisted of a number of fully laminar and non-reacting test cases that are among many that have been conducted experimentally in the hypersonic facilities at CUBRC.[4] A series of numerical studies were presented in that exercise, using either NS methods[5,6] or the DSMC method[7,8] , or both.[9] The comparisons of pressure coefficient and heat transfer Stanton number along the cone surface between numerical and experimental data were compiled in Ref. 10.

A general impression observed from Ref. 10 is that the NS methods consistently over predict the heat transfer on the fore cone ahead of where separation occurs while the DSMC solutions obtained by Boyd and Wang[8] show very good agreement with the measurements in the same region. Figure 2 shows that, ahead of separation, the NS solution has a heating rate about 20% higher than the DSMC solution which matches the experiment faithfully. The primary goal of this research is to find the reasons causing the differences between the NS and DSMC results. Note in Fig. 2 that the DSMC results do not accurately predict the size of the separation region.

Since DSMC needs a large amount of computational resources and time to reach a steady state solution for the double cone flow, it is more practical to deal with just a small portion of the first cone which is ahead of separation and is not influenced by shock/shock interaction. Only the region of $x/L < 0.6$ will be considered, where x is the axial distance from the cone tip and L is the length of the first cone (3.625″ in this study). We conduct several sensitivity tests for the DSMC method to verify that the solutions submitted in the code validation exercise are the best that our DSMC method can produce.

The layout of the paper is as follows. First, a brief description of the DSMC and NS methods currently employed is provided. Then, sensitivity test results for the DSMC computation of the sharp/blunted cone flows are presented. Flow field comparisons for DSMC and NS methods are also included. At the end, we assess the agreement between the computational solutions and experiment data. Some final thoughts will be given in the section of discussion and conclusions.

Numerical Methods

DSMC

The particular DSMC code, named MONACO, employed in this study was first developed by Dietrich and Boyd[11] in 1996. Since then, MONACO has been further modified and applied to a wide variety of rarefied gas problems. MONACO employs the Variable Soft Sphere (VSS) collision model,[12] the variable rotational energy exchange probability model of Boyd[13] and the variable vibrational energy exchange probability model of Vijayakumar *et al.*.[14] Cell weighting factors and time-steps may be set uniquely for each cell in the grid. A sub-cell scheme is implemented for selection of collision pairs where the number of subcells is scaled by the local mean free path.

Navier-Stokes

The NS calculations are performed with an implicit finite-volume CFD code based on the methods discussed in Refs. 1, 5. The fluxes are evaluated with a second-order accurate flux-vector splitting method based on a modified Steger-Warming method.[15,16] The slip boundary conditions were implemented in the approach presented by Gökcen:[17]

$$\vec{u}_s = \frac{2-\sigma_v}{\sigma_v}\lambda_v \frac{\partial \vec{u}}{\partial n}\Big|_w \quad (1)$$

$$T_s = T_w + \frac{2-\sigma_T}{\sigma_T}\lambda_T \frac{\partial T}{\partial n}\Big|_w . \quad (2)$$

T_w is the temperature of the surface and σ_v and σ_T are the tangential momentum and thermal accommodation coefficients of the surface. Here the mean free path for momentum, λ_v, and thermal energy, λ_T are defined as

$$\lambda_v = \frac{2\mu}{\rho \bar{c}}, \qquad \lambda_T = \frac{2\kappa}{\rho \bar{c} c_v}$$

where μ and κ are the viscosity and thermal conductivity. $\bar{c} = \sqrt{8RT/\pi}$ is the mean molecular speed, and c_v is the specific heat at constant volume. The subscript w indicates conditions at the wall, or surface of the wind tunnel model. The slip velocity is tangent to the surface, and the normal-direction velocity component is set to zero at the surface.

Once the slip temperature is computed, heat flux to the surface is calculated as

$$q_w = \kappa \frac{\partial T}{\partial n}\Big|_w = \kappa \frac{T_1 - T_s}{\Delta n}$$

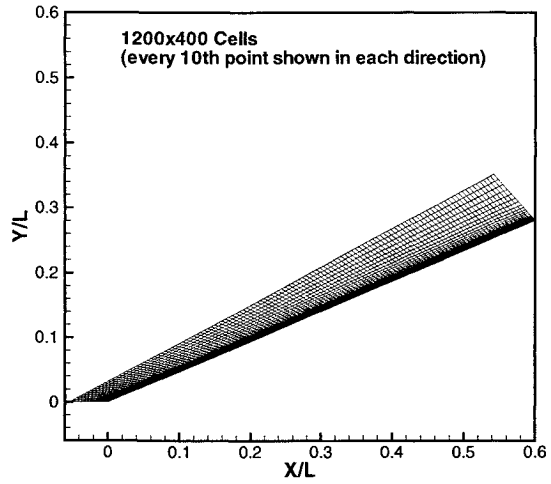

Fig. 3 Grid employed for 25° sharp cone.

where T_1 is the temperature at the first cell center away from the wall, and Δn is the normal-direction distance from that cell center to the surface.

DSMC Results

The fluid is pure nitrogen and the free stream conditions considered are listed in Table 1. The accommodation coefficient (σ) is 0.85 in all computations unless otherwise stated. The Run numbers refer to the experiments performed in CUBRC.[4]

Table 1 Free stream conditions for the 25-55° double cone flows.

	Run 35	Run 31
M_∞	11.3	11.3
Re_L (10^3)	14.5	13.2
T_∞ (K)	138.9	144.4
T_{wall} (K)	296.1	297.2
V_∞ (m/s)	2712.2	2764.5
ρ_∞ (10^{-3}kg/m^3)	0.552	0.511

Run 35

The configuration employed in Run 35 is a sharp 25° half-angle cone as depicted in Fig. 1. The finest structured grid, 1200 cells along the body by 400 cells normal to the body, used in our computations is shown in Fig. 3. It has increased cell density near the cone tip and cone surface in order to resolve the locally high gradients.

A reference time step of 10^{-9} sec is employed for the first 0.1 msec of the calculations. After that, the time step is doubled. The total number of particles in each grid is about 20 times the total number of the cells. The results presented below are obtained by sampling over a period of 0.02 msec.

Grid Sensitivity

In this section, we examine the computed surface quantities at different levels of grid refinement. The two surface quantities considered are pressure coefficient and Stanton number:

$$C_p = \frac{p - p_\infty}{\frac{1}{2}\rho_\infty V_\infty^2}, \qquad St = \frac{q_w}{\frac{1}{2}\rho_\infty V_\infty^3}$$

and they are plotted versus the normalized axial distance.

In Fig. 4, the surface pressure coefficient and Stanton number are shown at 0.2 msec. It is clear that the 600×400 grid under predicts the surface pressure coefficient near the cone tip although its heat transfer result is close to the others. We believe the 1200×400 grid yields reliable solutions in terms of grid sensitivity and thereafter use it for the further studies of this case.

Time Convergence

Figure 5 shows the surface pressure coefficient and Stanton number at 0.1, 0.2 and 0.3 msec. We can easily see that the flow does not reach the steady state until at least about 0.2 msec and therefore it is safe to take 0.3 msec as the time required for the flow to reach steady state.

Accommodation Coefficient

The surface pressure coefficient and Stanton number computed with two different accommodation coefficients are displayed in Fig. 6. It is indicated that only minor differences are observed. From this study, we conclude that the DSMC results are insensitive to σ in the range from 0.85 to 1.0.

Numerical Parameter Studies

A fundamental assumption for DSMC is that particle motion and particle collisions can be decoupled. This assumption requires that the simulation time-step (Δt) be smaller than the local mean collision time (τ). In addition, we are able to randomly select the colliding particles in a cell while ignoring their positions if the computational cell size (Δs) is smaller than the local mean free path (λ), statistically speaking. In other words, we need $\Delta t/\tau < 1$ and $\Delta s/\lambda < 1$. To study the numerical parameters employed, data have been extracted vertically along six different x-coordinates: x/L = 0.0, 0.1, 0.2, 0.3, 0.4, and 0.5. Figure 7 shows the ratio of the simulation time-step to the local mean collision time. It is evident that the simulation time-step criterion is satisfied everywhere.

The characteristic cell size in our grid, Δs, is determined by the length scale of the cell in the direction of the maximum gradient of density, pressure, temperature or velocity and its ratio to the local mean free path is shown in Fig. 8. The cell size criterion is generally satisfied, except in the shock region in some places. Even in the worst condition, the cell size is no

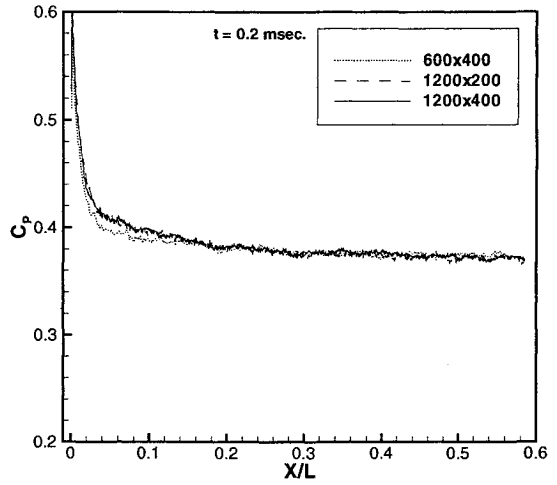

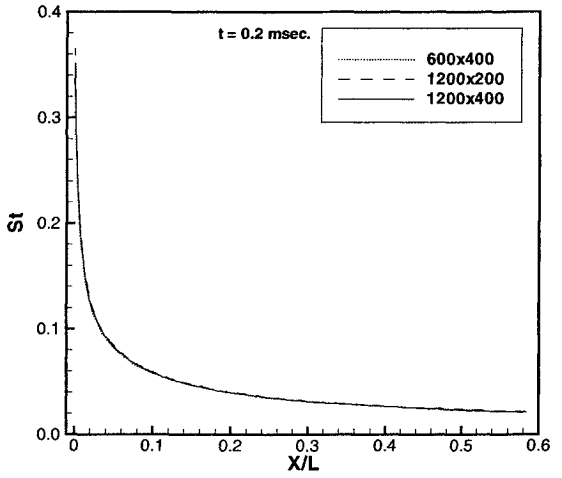

Fig. 4 Surface pressure and heat transfer coefficients at different levels of grid refinement for 25° sharp cone.

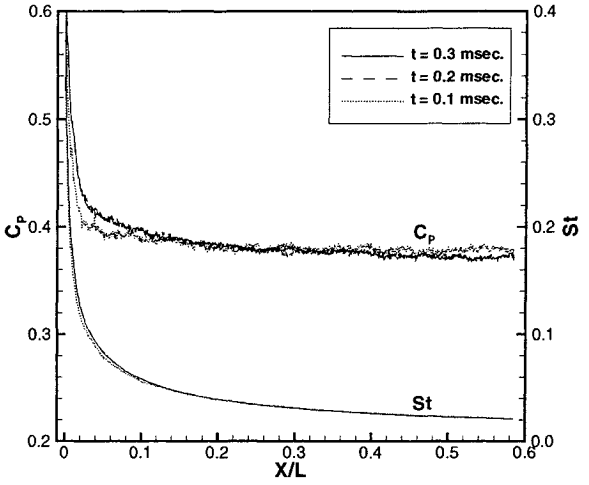

Fig. 5 Surface pressure and heat transfer coefficients at different times for 25° sharp cone (1200×400 grid).

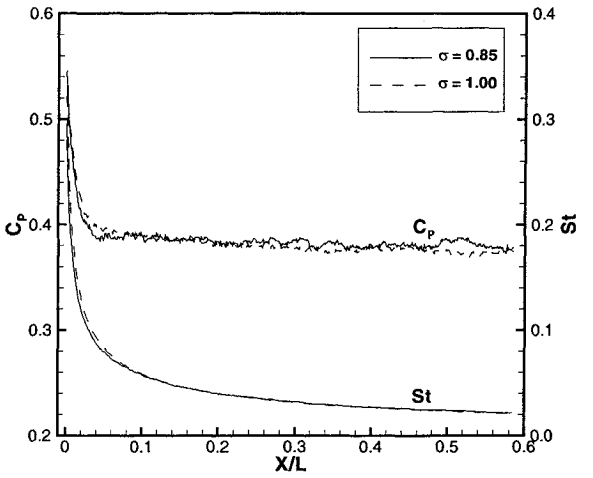

Fig. 6 Surface pressure and heat transfer coefficients with σ = 0.85 and 1.0 for 25° sharp cone (1200×400 grid).

more than twice the local mean free path. In addition, there are a large number of particles per cell in the shock region as shown in Fig. 9, and therefore the use of the sub-cell scheme should provide adequate spatial resolution. It is important to note that the criteria for Δt and Δs are met within the boundary layer, which gives us confidence with our solutions in the vicinity of the cone surface.

DSMC and CFD Comparisons

Profiles of velocity and translational temperature at three different locations for both numerical results are shown in Fig. 10, with the definition of δn as the normal-distance from the surface. It is clear that the CFD method has generated a thinner and stronger shock wave. The translational temperature predicted by the DSMC method overshoots right after the shock that is likely a result of the nonequilibrium with the rotational energy mode.

Detailed profiles near the surface are plotted in Fig. 11. The maximum δn was chosen to be much smaller than the boundary layer thickness (see Fig. 10(a)). We can see that the velocity predicted by the CFD slip boundary conditions are a little higher than the DSMC solutions on the surface but it increases slower in the normal direction and eventually is less than the DSMC velocity. The translational temperature calculated by CFD in general is also higher on the surface. The difference at $x/L = 0.1$ reaches about 25%.

The temperature gradients evaluated by taking the

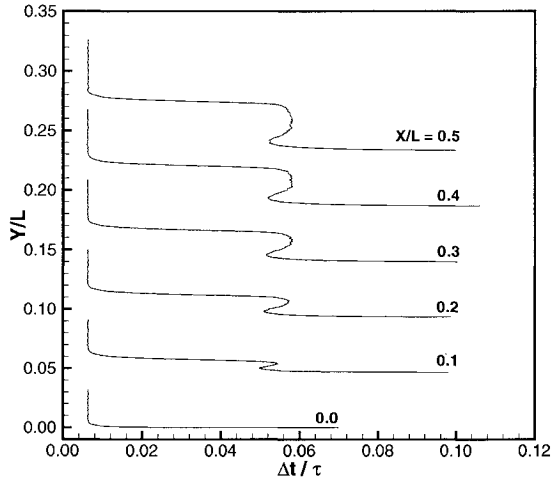

Fig. 7 Ratio of simulation time-step to local mean collision time along six different constant-x coordinates.

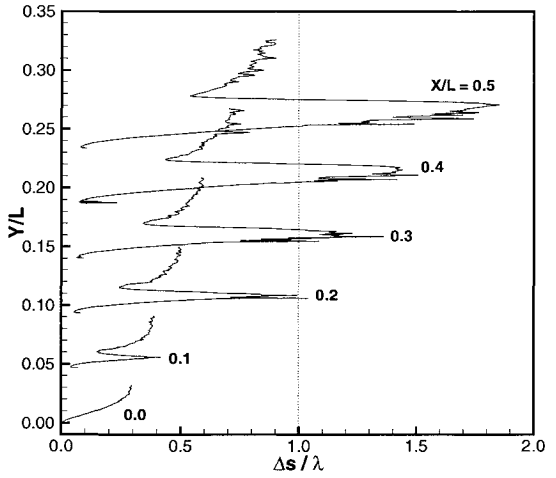

Fig. 8 Ratio of simulation cell size in direction of maximum gradient to local mean free path along six different constant-x coordinates.

first derivative of the temperature profile at the surface are shown in Fig. 12. It is clear that there is a significant difference of temperature gradient near the leading edge. It should be caused by the different schemes employed by the DSMC and CFD to calculate the energy modes. At the leading edge where' nonequilibrium effects are strong, the assumption of thermal equilibrium for the Navier-Stokes equations breaks down. Therefore, it is normal for DSMC and CFD to provide different results near the leading edge. When the flow goes downstream, the nonequilibrium effects gradually disappear. The flow field properties from the two numerical methods then become similar.

We present another approach to look at the nonequi-

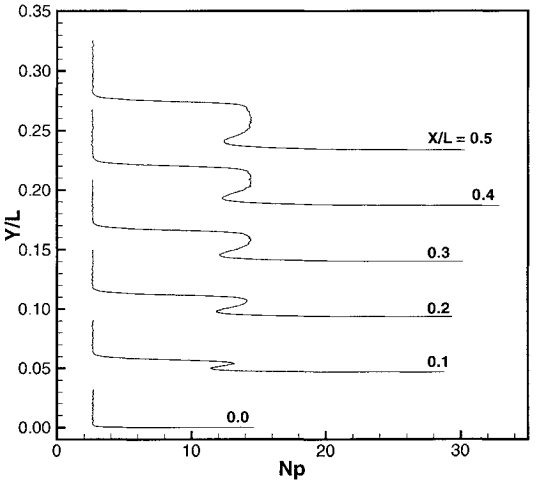

Fig. 9 Number of particles per cell along six different constant-x coordinates.

librium effect. In our DSMC calculations, we sample the velocity components in the Knudsen layer at several locations. Figure 13 plots the normalized velocity distribution function in the direction parallel (denoted by $\|$) and perpendicular (denoted by $\perp$) to the surface. It is evident that the velocity distribution function in the two directions deviates from the Maxwell-Boltzmann distribution to some extent. Figure 14 shows the corresponding translational temperatures. The translational temperature in the azimuth direction and the total translational temperature are also shown. We can conclude that there is strong thermal nonequilibrium near the cone tip.

Computation and Experiment Comparisons

Now, let us compare the two numerical results with the measured data. Figures 15 and 16 display the distributions of surface pressure coefficient and Stanton number for DSMC and CFD, and the experimental data. There are three curves for the CFD in each figure: the results obtained with a no-slip surface boundary condition, the slip boundary conditions as mentioned above, and the slip boundary conditions using T_{avg} that will be explained below. It is shown that the DSMC and the CFD with either slip boundary conditions provide results that are in agreement with the experimental data. The agreement of DSMC, CFD and the experiment suggests that the solutions submitted by Boyd and Wang[8] in the code validation exercise appear to be correct on the fore cone ahead of separation.

The expressions of slip boundary conditions, (1) and (2), used in the CFD are derived assuming only slow variations of the temperature in the vicinity of the surface.[17-19] However, the predicted slip velocity and temperature are very sensitive to the temperature used to evaluate the mean free paths, λ_v and λ_T. This

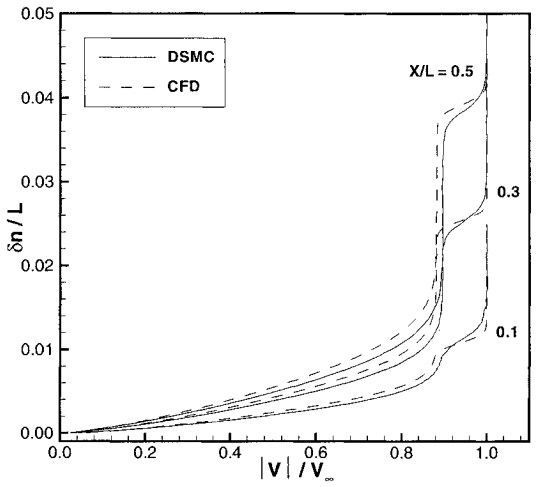

a) Non-dimensional velocity magnitude profiles (V/V_∞).

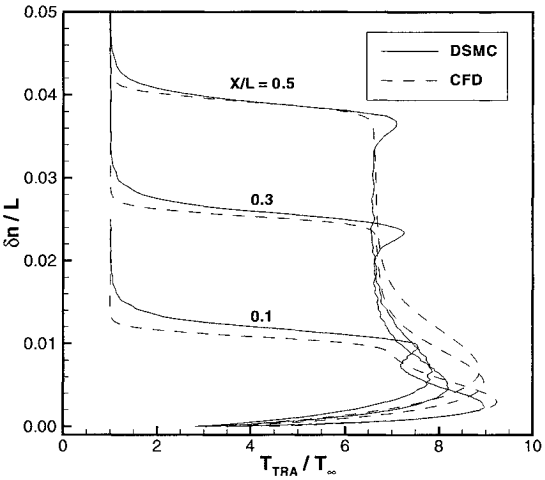

b) Non-dimensional translational temperature profiles (T_{tra}/T_∞).

Fig. 10 Profiles along the direction normal to the surface.

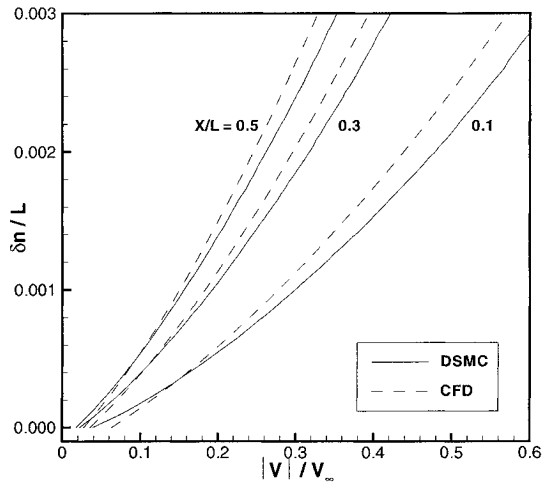

a) Non-dimensional velocity magnitude profiles (V/V_∞).

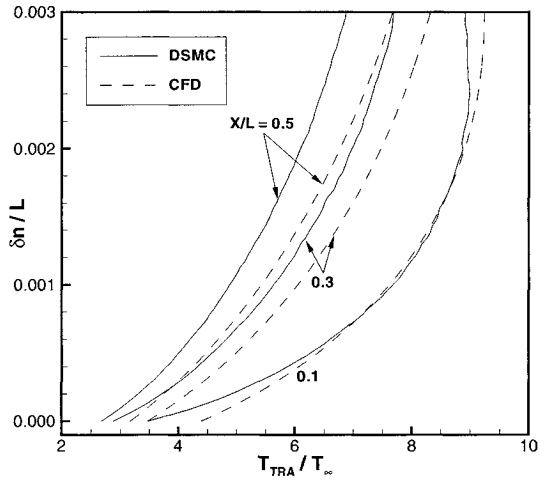

b) Non-dimensional translational temperature profiles (T_{tra}/T_∞).

Fig. 11 Close-up profiles along the direction normal to the surface.

can be seen by assuming that the pressure is constant normal to the surface in the Knudsen layer. Then for example, λ_v is

$$\lambda_v = \frac{2\mu}{\rho\bar{c}} = \frac{2\mu RT}{p\sqrt{8RT/\pi}} = \frac{\mu}{p}\sqrt{\frac{\pi RT}{2}}.$$

For a typical diatomic gas with the viscosity proportional to T^n, with $n = 0.7$ say, we have $\lambda_v \propto T^{n+\frac{1}{2}} \simeq T^{1.2}$. Similarly for λ_T. In the cone flow near the tip, the slip temperature can be more than twice the wall temperature. Thus, in our case with a rapidly varying temperature field, the temperature used to evaluate λ is critical to an accurate prediction of u_s and T_s for the CFD method.

In the Knudsen layer, there are two types of particles: those that enter the Knudsen layer from the outer stream, and those that reflect from the wall and are partially accommodated to the wall conditions. With the highly cooled wall, the former tend to be hot and the latter cold. The slip temperature characterizes the gas at the surface where these two types of molecules mix. Thus T_s is an appropriate temperature to use to evaluate λ_v and λ_T for CFD. However, this is certainly not a unique choice and the kinetic theory derivation of the slip condition does not provide guidance for any other choice. Similarly, the temperature used to evaluate κ in the heat transfer expression has a very large effect on the predicted heat transfer rate. Again,

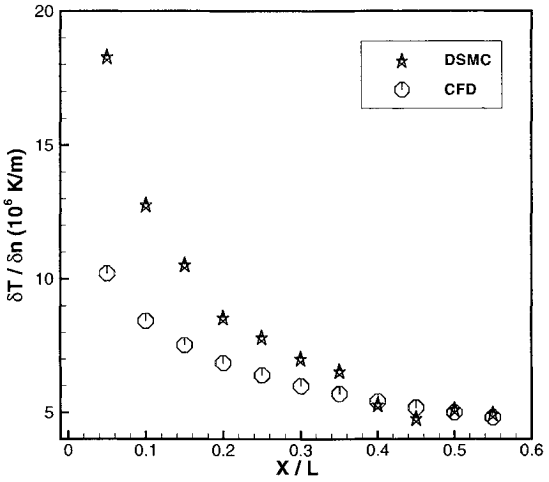

Fig. 12 Temperature gradients from DSMC and CFD solutions.

it makes sense to use the same temperature used to evaluate the mean free paths to evaluate the thermal conductivity.

For CFD, if we use accommodation coefficients, σ_v and σ_T, of 0.85 as used in the DSMC calculations, we find that using T_s to evaluate λ_v, λ_T, and κ results in an underpredicition of the slip temperature, and a resulting overprediction of the heat transfer rate. This is shown in Fig. 16, along with the prediction using a no-slip surface boundary condition.

We find that if we use a temperature given by

$$T_{avg} = \frac{2}{3}T_s + \frac{1}{3}T_w$$

to evaluate the mean free paths and the conductivity, we obtain excellent agreement with the experiments and the DSMC calculations. At this point, there is no justification for the use of this governing temperature. A more detailed derivation of the surface slip conditions including temperature variation must be performed to determine whether there is any physical basis for this result.

Run 31

The configuration in this case is basically the same as in Run 35 except that the cone has a blunted nose of 0.25″ in radius. The finest grid employed is shown in Fig. 17 for every 10th point in each direction. Flow particles near the stagnation point in this case are expected to undergo a lot of collisions. In addition, the flow will accelerate and expand around the blunted nose.

All numerical parameters are the same as in Run 35.

Grid Sensitivity

The surface pressure coefficient and Stanton number at 0.2 msec are shown in Fig. 18. The surface pressure

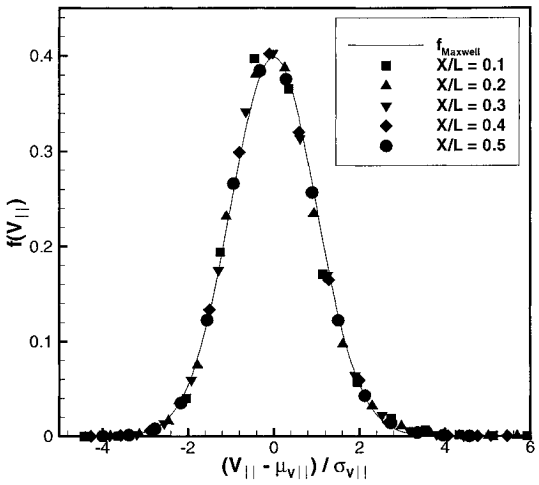

a) Velocity distribution function in the direction parallel to the cone surface.

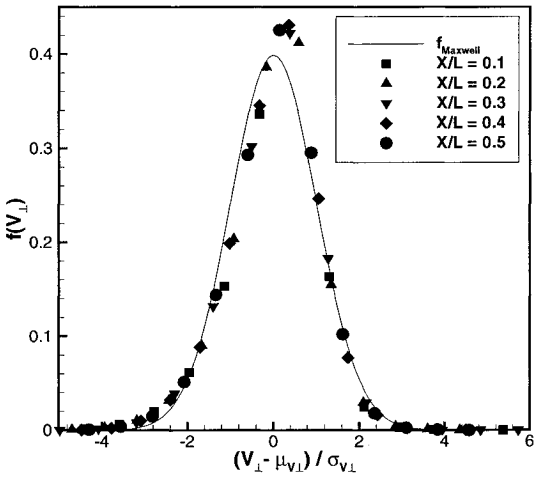

b) Velocity distribution function in the direction perpendicular to the cone surface.

Fig. 13 Velocity distribution function in the Knudsen layer at five different locations.

reaches the minimum value at about $x/L = 0.2$ and then increases further downstream. There are just minor differences between the results of the three grids employed. Hence, we use the 1200×400 grid for the further studies of this case.

Time Convergence

In Fig. 19, the surface pressure coefficient and Stanton number at 0.1, 0.2 and 0.3 msec are shown. As in the case of Run 35, we conclude that the flow does not approach to steady state before about 0.3 msec.

Numerical Parameter Studies

We performed the numerical parameter studies in the same way as in the previous case. As illustrated

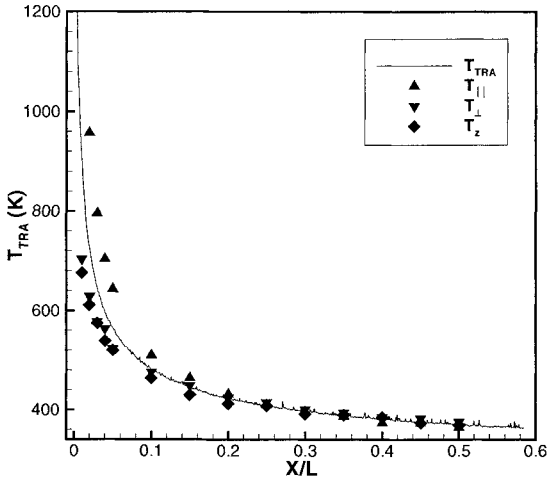

Fig. 14 Translational temperature in the Knudsen layer in $\|$, $\perp$ and z directions.

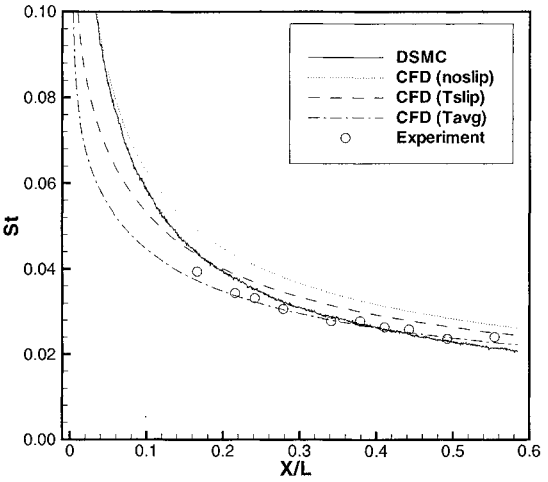

Fig. 16 Comparison of surface heat transfer coefficient.

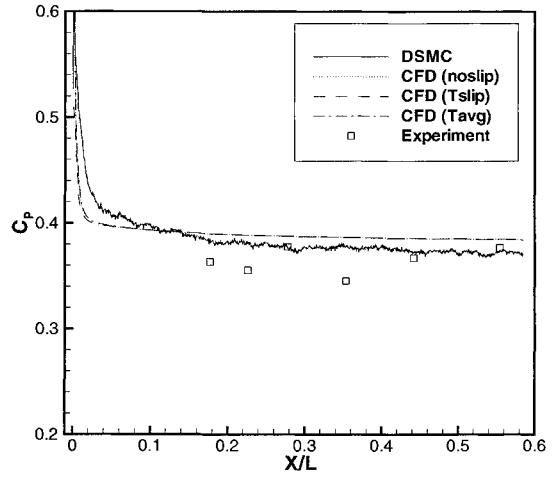

Fig. 15 Comparison of surface pressure coefficient.

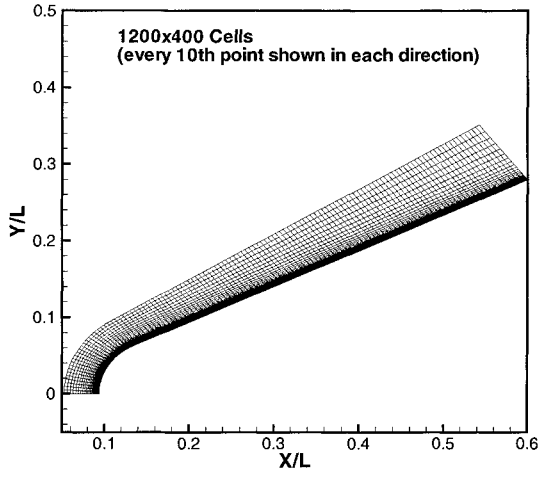

Fig. 17 Grid employed for 25° blunted cone.

in Fig. 20, the time-step criterion, $\Delta t/\tau < 1$, is satisfied everywhere. The computational cell size generally meets the requirement, $\Delta s/\lambda < 1$. For any places where the cell size criterion fails, a large number of particles per cell (Fig. 22) and the sub-cell scheme work together to provide good resolution as mentioned above.

DSMC and NS Comparisons

We compare the velocity and temperature profiles of the two numerical results. Similar to the case of Run 35, the velocity profiles in Fig. 23(a) show that the CFD method generates a thinner and stronger shock, and the DSMC method overshoots the translational temperature in Fig. 23(b) right after the shock because of nonequilibrium with the rotational energy mode.

The profiles very close to the surface are shown in Fig. 24. We can see that both the temperature and velocity evaluated by the CFD with the slip boundary conditions are higher than the DSMC results on the surface.

A significant difference of temperature gradient near the nose stagnation point still can be observed in Fig. 25, although there are a lot of collisions taking place in that region. The translational temperatures in the Knudsen layer in the parallel and perpendicular directions to the surface and the azimuth direction in Fig. 26 indicate that the flow field in the Knudsen layer may be nonequilibrium along the entire cone.

Computation and Experiment Comparisons

Finally, the comparisons of the numerical results and experimental data are displayed in Figs. 27 and 28. For the surface pressure coefficient, the DSMC results

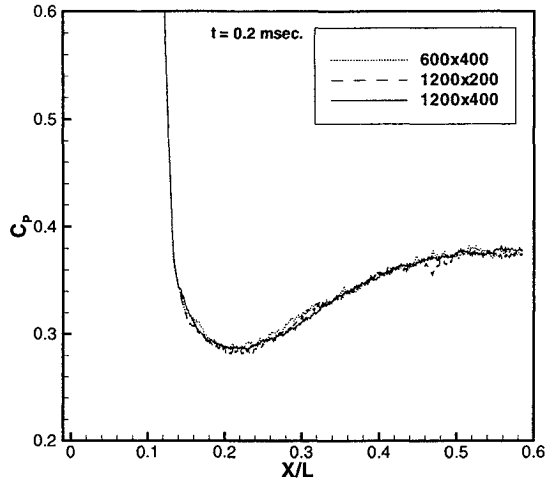

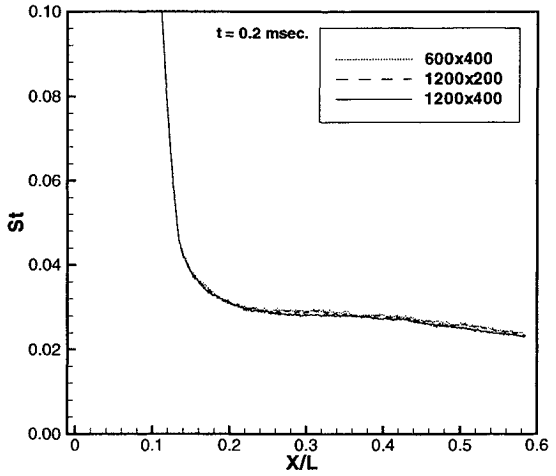

Fig. 18 Surface pressure and heat transfer coefficients at different levels of grid refinement for 25° blunted cone.

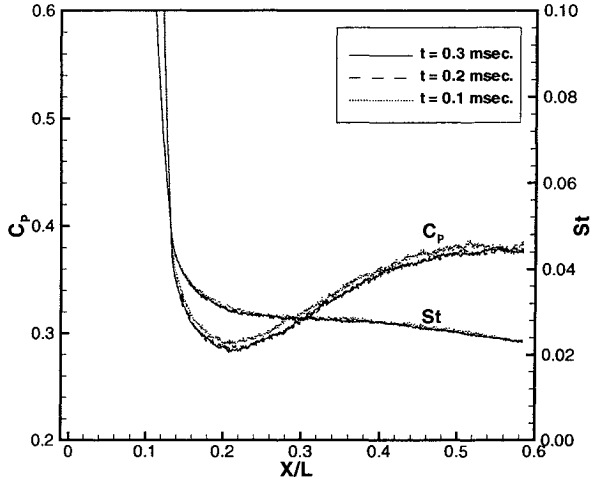

Fig. 19 Surface pressure and heat transfer coefficients at different times for 25° blunted cone (1200×400 grid).

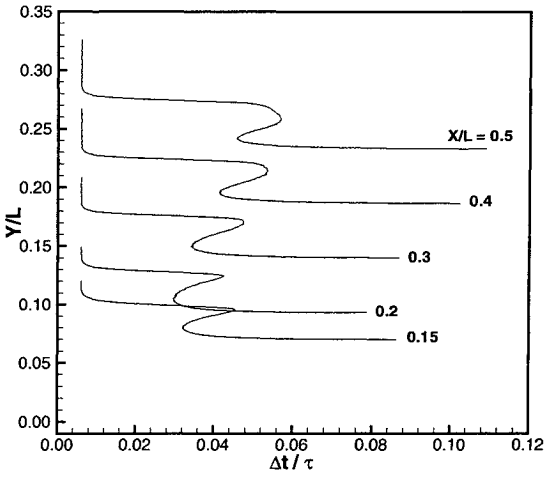

Fig. 20 Ratio of simulation time-step to local mean collision time along five different constant-x coordinates.

are slightly closer to the measured data. The Stanton number calculated by the CFD method using a no-slip surface boundary condition or the slip boundary conditions of T_s is higher than the experimental data while the DSMC method and the CFD method using the slip boundary conditions of T_{avg} give an excellent prediction.

Discussion and Conclusions

We have conducted an extensive numerical investigation of hypersonic flow over axisymmetric sharp and blunted cones using the DSMC and CFD methods. For the DSMC method, the results are not sensitive to increasing cells in the direction normal to the surface if the number of cells parallel to surface is at least 1200. It takes about 0.3 msec for the flow to reach a steady state. The results are also not sensitive to the accommodation coefficient.

For the CFD method, we find that the predicted heat transfer rate largely depends on the temperature used to evaluate the mean free path and the thermal conductivity in the slip boundary conditions. Besides, given the fact that the slip boundary conditions employed in this study only allows slow variations of the temperature in the vicinity of the surface and that there is rapid temperature change in that region for the flows considered, it is possible that higher order terms are required to describe the flow and surface phenomena. The use of T_{avg} to evaluate λ and κ has no physical justification although it performs very well in our research.

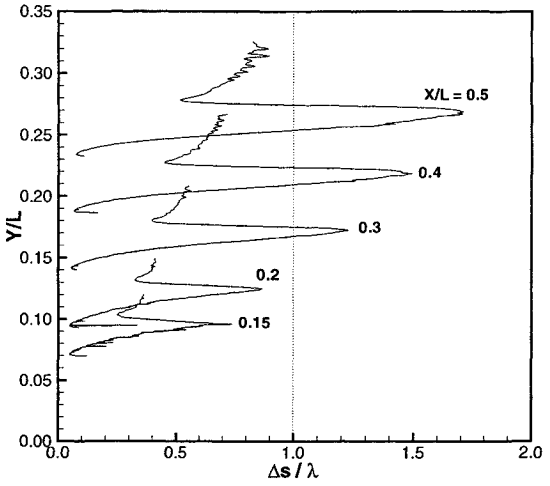

Fig. 21 Ratio of simulation cell size in direction of maximum gradient to local mean free path along five different constant-x coordinates.

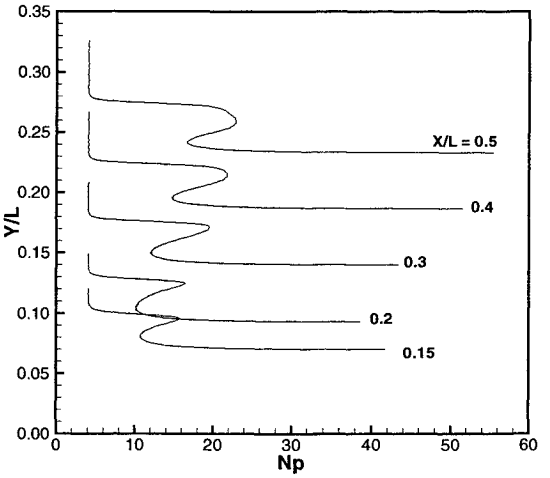

Fig. 22 Number of particles per cell along five different constant-x coordinates.

The comparison of the DSMC and CFD results shows that the shock calculated by CFD is thinner and stronger.

The velocity distribution function calculated in the Knudsen layer by the DSMC method demonstrates a strong nonequilibrium effect near the sharp cone tip or over the entire blunted cone. It raises a question to the accuracy of the computational methods based on the Navier-Stokes equations that assume the flow is close to equilibrium everywhere.

Acknowledgments

Funding for this work was provided by the Air Force Office of Scientific Research under grant F49620–01–1-0003 with Dr. Steven Walker as technical monitor.

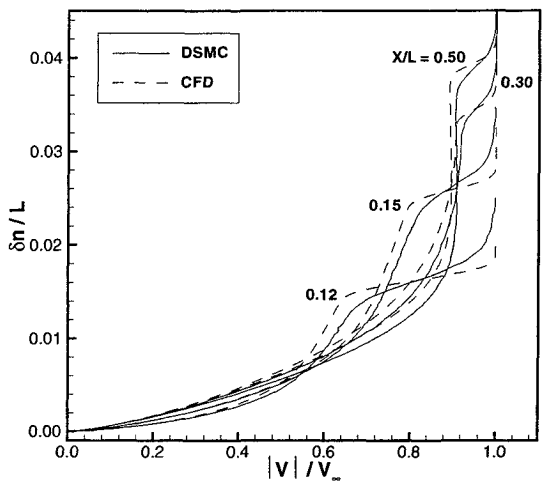

a) Non-dimensional velocity magnitude profiles (V/V_∞).

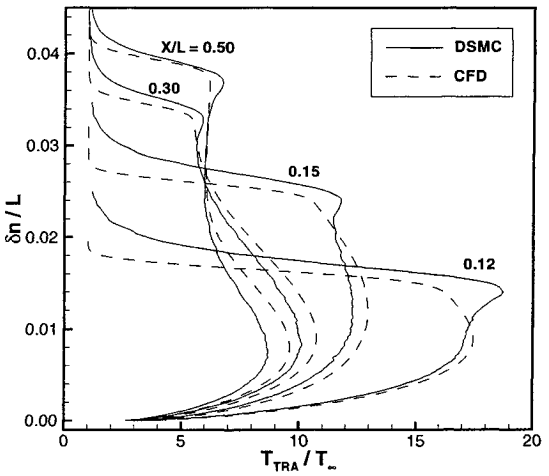

b) Non-dimensional translational temperature profiles (T_{tra}/T_∞).

Fig. 23 Profiles along the direction normal to the surface.

Computer resources on the IBM-SP machine at the Minnesota Supercomputing Institute are gratefully acknowledged.

References

[1]Candler, G. V., Nompelis, I., and Holden, M. S., "Computational Analysis of Hypersonic Laminar Viscous-Inviscid Interactions," AIAA Paper 2000–0532, Jan. 2000.

[2]Moss, J. N., "DSMC Simulation of Shock Interactions About Sharp Double Cones," NASA TM–2000–210318, Aug. 2000.

[3]Bird, G. A., *Molecular Gas Dynamics and the Direct Simulation of Gas Flows*, Oxford University Press, Oxford, 1994.

[4]Holden, M. S., "Experimental Database from CUBRC Studies in Hypersonic Laminar and Turbulent Interacting Flows including Flowfield Chemistry," RTO Code Validation of DSMC

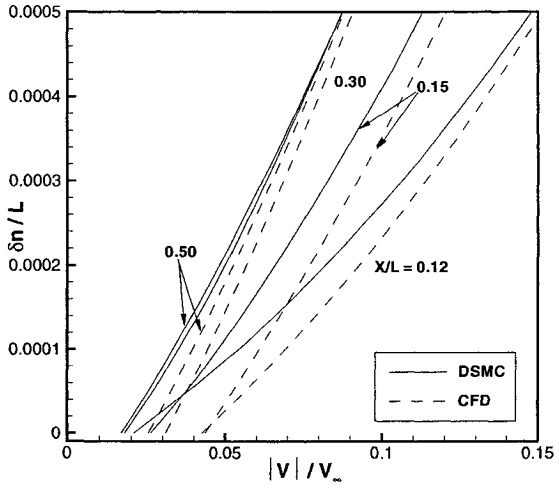

a) Non-dimensional velocity magnitude profiles (V/V_∞).

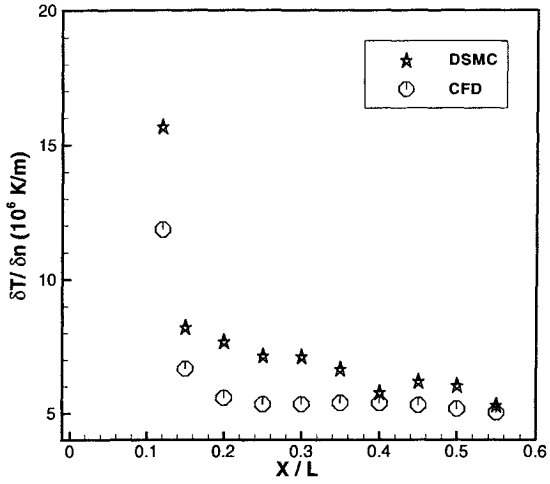

Fig. 25 Temperature gradients from DSMC and CFD solutions.

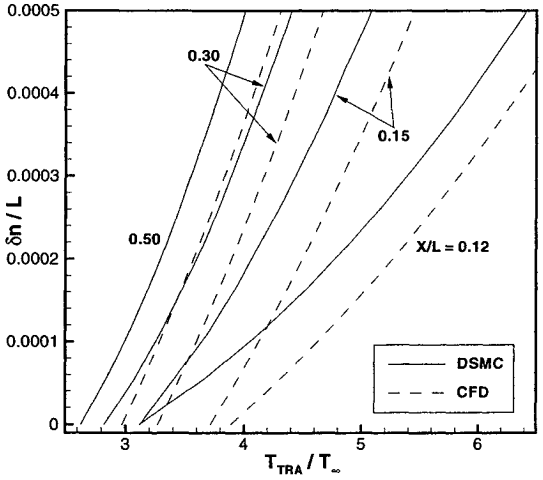

b) Non-dimensional translational temperature profiles (T_{tra}/T_∞).

Fig. 24 Close-up profiles along the direction normal to the surface.

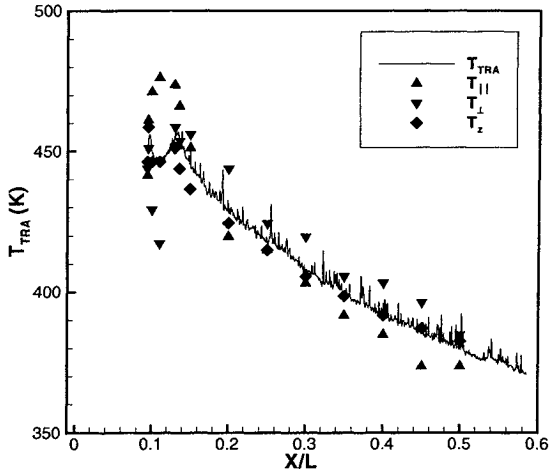

Fig. 26 Translational temperature in the Knudsen layer in ||, ⊥ and z directions.

and Navier-Stokes Code Validation Studies CUBRC Report, June 2000.

[5]Candler, G. V., Nompelis, I., and Druguet, M.-C., "Navier-Stokes Predictions of Hypersonic Double-Cone and Cylinder-Flare Flow Field," AIAA Paper 2001–1024, Jan. 2001.

[6]Gnoffo, P. A., "CFD Validation Studies for Hypersonic Flow Prediction," AIAA Paper 2001–1025, 2001.

[7]Moss, J. N., "DSMC Computations for Regions of Shock/Shock and Shock/Boundary Layer Interaction," AIAA Paper 2001–1027, Jan. 2001.

[8]Boyd, I. D. and Wang, W.-L., "Monte Carlo Computations of Hypersonic Interacting Flows," AIAA Paper 2001–1029, Jan. 2001.

[9]Roy, C. J., Bartel, T. J., Gallis, M. A., and Payne, J. L., "DSMC and Navier-Stokes Predictions for Hypersonic Laminar Interacting Flows," AIAA Paper 2001–1030, Jan. 2001.

[10]Harvey, J. K., Holden, M. S., and Wadhams, T. P., "Code Validation Study of Laminar Shock/Boundary Layer and Shock/Shock Interactions in Hypersonic Flow. Part B: Comparison with Navier-Stokes and DSMC Solutions," AIAA Paper 2001–1031, Jan. 2001.

[11]Dietrich, S. and Boyd, I. D., "Scalar and Parallel Optimized Implementation of the Direct Simulation Monte Carlo Method," *Journal of Computational Physics*, Vol. 126, 1996, pp. 328–342.

[12]Koura, K. and Matsumoto, H., "Variable Soft Sphere Molecular Model for Air Species," *Physics of Fluids A*, Vol. 4, No. 5, May 1992, pp. 1083–1085.

[13]Boyd, I. D., "Analysis of Rotational Nonequilibrium in Standing Shock Waves of Nitrogen," *AIAA Journal*, Vol. 28, 1990, pp. 1997–1999.

[14]Vijayakumar, P., Sun, Q., and Boyd, I. D., "Detailed Models of Vibrational-Translational Energy Exchange for the Direct Simulation Monte Carlo Method," *Physics of Fluids*, Vol. 11, No. 8, Aug. 1999, pp. 2117–2126.

[15]MacCormack, R. W. and Candler, G. V., "The Solution of the Navier-Stokes Equations Using Gauss-Seidel Line Relax-

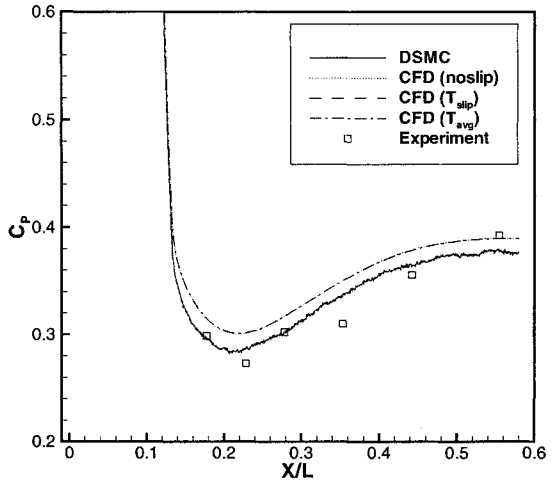

Fig. 27 Comparison of surface pressure coefficient.

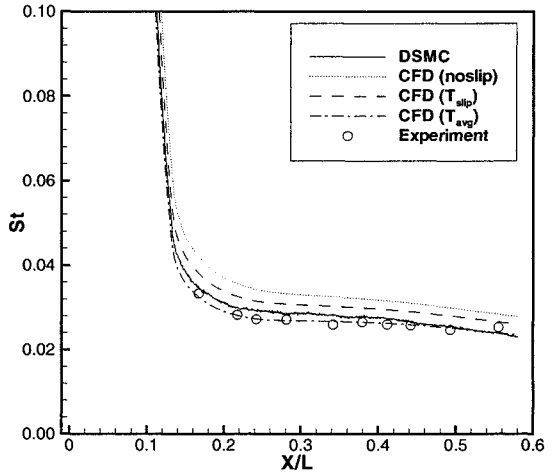

Fig. 28 Comparison of surface heat transfer coefficient.

ation," *Computers and Fluids*, Vol. 17, No. 1, 1989, pp. 135–150.

[16]Candler, G. V. and MacCormack, R. W., "The Computation of Hypersonic Ionized Flows in Chemical and Thermal Nonequilibrium," *Journal of Thermophysics and Heat Transfer*, Vol. 5, No. 3, 1991, pp. 266–273.

[17]Gökcen, T. and MacCormack, R. W., "Nonequilibrium Effects for Hypersonic Transitional Flows Using Continuum Approach," AIAA Paper 1989–0461, Jan. 1989.

[18]Gombosi, T. I., *Gaskinetic Theory*, Cambridge University Press, 1994.

[19]Schaaf, S. A. and Chambre, P. L., *Flow of Rarefied Gases*, Princeton University Press, Princeton, 1958.